

## AN OVERALL ASSESSMENT OF ABND MODEL FOR LARGE-SCALE BUBBLY FLOWS

Xinyue DUAN<sup>1,2</sup>, Sherman C.P. CHEUNG<sup>2</sup>, Guan H. YEOH<sup>3</sup>, Jiyuan TU<sup>2\*</sup>,  
 Eckhard KREPPER<sup>4</sup>, Dirk LUCAS<sup>4</sup>

<sup>1</sup> Institute of Refrigeration and Cryogenic Eng., Xi'an Jiaotong University, Xi'an, P.R.710049, China

<sup>2</sup> School of Aerospace, Mechanical and Manufacturing Engineering, RMIT University, VIC 3083, Australia

<sup>3</sup> Australian Nuclear Science and Technology Organization (ANSTO), NSW 2234, Australia

<sup>4</sup> Institute of Safety Research, Forschungszentrum Rossendorf e.V., Desden 01314, Germany

\*Corresponding author, E-mail address: Jiyuan.TU@rmit.edu.au

### ABSTRACT

For increasing the predictability of equipment and improving efficiency of production, there is a high demand to develop a compact and efficient mathematical model capable of modelling the complex bubbly flow structures which frequently occur in large-scale industrial engineering systems. A generalized Average Bubble Number Density (ABND) transport equation model in conjunction with three forms of bubble coalescence and breakage kernels was implemented and incorporated into commercial software ANSYS CFX 11. The main focus of this paper is to assess the overall performance of the ABND model and the three different bubble mechanism kernels under a large-scale gas-liquid bubbly flow system. Based on the high-quality TOPFLOW database for air-water two-phase flows in a large vertical pipe with nominal diameter of 195.3mm, experimental data were strategically selected for model validation. To examine the relative merits and drawbacks of three forms of coalescence and breakage kernels, model predictions of local radial distributions of bubble rise velocity, volume fraction and bubble size were compared against experimental results. The capabilities in predicting the "core peak" volume fraction profiles and evolution process of bubble rise of different kernels were discussed.

### NOMENCLATURE

$C_{RC}$	Random collision coefficient
$C_{TI}$	Turbulent impact coefficient
$C_{WE}$	Wake entrainment coefficient
$C_{RC1}C_{RC2}C_{RC3}$	Adjustable model constants for coalescence sources
$C_{TI1}C_{TI2}$	Adjustable model constants for breakage sources
$C_{WE}$	Adjustable model constants for wake entrainment sources
$D_s$	Bubble Sauter mean diameter
$F_C$	Calibration factor for coalescence
$F_B$	Calibration factor for breakage
$n$	Average number density of gas phase
$Re$	Flow Reynolds number
$\mu_g$	Gas velocity vector
$We$	Weber number
$We_{cr}$	Critical Weber number

### Greek Symbols

$\alpha$	Gas volume fraction
$\alpha_{max}$	Maximum allowable volume fraction

$\varepsilon$	Turbulence kinetic energy dissipation
$\mu_e$	Effective viscosity
$\rho$	Density
$\sigma$	Surface tension
$\varphi_n^{RC}$	Bubble number density change rate due to random collision
$\varphi_n^{TI}$	Bubble number density changes rate due to impact of turbulent eddies
$\varphi_n^{WE}$	Bubble number density changes rate due to wake entrainment

### INTRODUCTION

Large scale gas-liquid bubbly flows with high Reynolds number are featured in various industrial and mineral systems where complex multiphase flow structures are inherently embedded. For safety analysis or design optimization, reliable predictions of the volume fraction distribution and other two-phase flow parameters are of paramount importance.

Recently, population balance (PB) approach has been considered as one of the efficient algorithm for solving the evolution processes of gas-liquid flows (Chen et al., 2005; Ekambara and Dhotre, 2007; Cheung et al., 2008). In our previous study (Cheung et al., 2007), a ABND model were introduced as a compact and efficient population balance modelling approach for solving practical gas-liquid bubbly flows. Nonetheless, in large-scale bubble columns, wide range of bubble size is commonly exist due to the rigorous breakage and coalescence processes. These processes modify the size and shape of the dispersed phase introducing complex hydrodynamic behaviour of the system. To extend the population balance modelling for solving large-scale gas-liquid systems, the strong coalescence and breakage effects due to the interactions among bubbles and between bubbles and turbulent eddies should be properly addressed. One of the semi-empirical models of bubble coalescence and bubble breakage that has been widely cited is the model developed by Wu et al. (1998). However, some experimental observations have suggested that coalescence due to wake entrainment is only significant between pairs of large cap bubbles and the fluid is sufficiently viscous to maintain their wake laminar (Serizawa and Kataoka, 1988). Furthermore, bubble expansion due to static pressure drop along vertical pipe was not considered in the model. To circumvent this problem, Hibiki and Ishii (2002) developed another kernel model which included gas expansion term and omitted wake entrainment effect from bubble coalescence. Lately,

Yao and Morel (2004) presented a novel model by considering both the free travelling time and the interaction time in evaluating the coalescence and breakage frequency.

In the present article, to explore the capability of ABND model in solving practical large scale bubbly flows, model predictions are strategically validated against the TOPFLOW experimental data with large pipe diameter presented by Prasser et al. (2007). The three aforementioned bubble mechanism kernels were incorporated into ABND transport equation to handle the source and sink of bubble number density due to coalescence and breakage processes. Model predictions of some important parameters; such as: local volume fraction profile, bubble diameter and gas velocity; were assessed and validated against the experimental data. Performance of the three different kernels in capturing the dynamical bubble size changes within the system was also discussed.

## MATHEMATICAL MODEL

### Two Fluid Model

Based on our previous study (Cheung et al., 2007), the two phase fluid motions are modeled through the two-fluid model based on Eulerian-Eulerian framework. In isothermal flow condition, with no interfacial mass transfer, the continuity equation of the two-phases is written as (Ishii, 1975; Drew and Lahey, 1979):

$$\frac{\partial(\rho_i \alpha_i)}{\partial t} + \nabla \cdot (\rho_i \alpha_i \bar{u}_i) = 0 \quad (1)$$

where  $\alpha$ ,  $\rho$  and  $\bar{u}$  is the gas volume fraction, density and velocity of each phase. The subscripts  $i=1$  or  $g$  denotes the liquid or gas phase.

The momentum equation for the two-phase can be expressed as follow:

$$\frac{\partial(\rho_i \alpha_i \bar{u}_i)}{\partial t} + \nabla \cdot (\rho_i \alpha_i \bar{u}_i \bar{u}_i) = -\alpha_i \nabla P + \alpha_i \rho_i \bar{g} + \nabla \cdot [\alpha_i \mu_i^e (\nabla \bar{u}_i + (\nabla \bar{u}_i)^T)] + F_i \quad (2)$$

On the right hand side of (2),  $F_i$  represents the total interfacial force calculated with averaged variables.  $\bar{g}$  is the gravity acceleration vector and  $P$  is the pressure.

$$\begin{aligned} F_i &= F_{lg} = -F_{gl} \\ &= F_{lg}^{\text{drag}} + F_{lg}^{\text{lift}} + F_{lg}^{\text{lubrication}} + F_{lg}^{\text{dispersion}} \end{aligned} \quad (3)$$

Here,  $F_{gl}$  denotes the momentum transfer terms from the gas phase to the liquid phase and vice versa for  $F_{lg}$ .  $F_{lg}^{\text{drag}}$  is the drag force between gas and liquid due to shear effects and is handled by the model by Ishii and Zuber (1979). Apart from the drag force, the non-drag forces acting on bubble are mainly comprised by the lift force  $F_{lg}^{\text{lift}}$ , the turbulent dispersion force  $F_{lg}^{\text{dispersion}}$  and the wall lubrication force  $F_{lg}^{\text{lubrication}}$  which act mostly in the lateral direction perpendicular to the flow. In summary, the lift force plays an important role on the de-mixing effect of small and large bubbles which consequentially contributes to the ‘‘wall peak’’ or ‘‘core peak’’ gas volume fraction distribution. The force can be correlated to the relative velocity and the local liquid vorticity by Tomiyama et al. (1998). The turbulent dispersion force considering the

turbulent mixing of the bubbles is modelled according to Antal et al. (1991). The wall lubrication force which considers the repelling effect of the wall on bubbles is described by the model of Burns et al. (2004).

### Average Bubble Number Density (ABND) Model

The Average Bubble Number Density (ABND) model as a simpler population balance approach is introduced to describe the bubble mechanism. The ABND transport equation based on the concept of population balance of dispersed bubbles is given by:

$$\frac{\partial n}{\partial t} + \nabla \cdot (\bar{u}_g n) = \phi_n^{RC} + \phi_n^{TI} + \phi_n^{WE} \quad (4)$$

where  $n$  is the average bubble number density,  $\phi_n^{RC}$ ,  $\phi_n^{TI}$  and  $\phi_n^{WE}$  are the bubble number density changes due to random collision, turbulent induced breakage and wake entrainment respectively which is the key parts of describing bubble ‘‘birth’’ and ‘‘death’’ rates. For closure of the transport equation, three forms of kernels proposed by Wu et al (1998), Hibiki and Ishii (2002) and Yao and Morel (2004) were adopted in the present study. A brief discussion is stated below.

### Wu et al. (1998) Model

Considering the characteristic times for binary collision and the mean traveling length between neighboring bubbles, Wu et al. (1998) proposed the random collision rates of bubble coalescence is given by:

$$\begin{aligned} \phi_n^{RC} &= -F_C C_{RC1} \frac{\alpha_g^2 \varepsilon^{1/3}}{D_S^{11/3} \alpha_{\max}^{1/3} (\alpha_{\max}^{1/3} - \alpha_g^{1/3})} \\ &\quad \left[ 1 - \exp\left(-\frac{C_{RC2} \alpha_{\max}^{1/3} \alpha_g^{1/3}}{\alpha_{\max}^{1/3} - \alpha_g^{1/3}}\right) \right] \end{aligned} \quad (5)$$

where  $C_{RC} = 0.021$ ,  $C_{RC2} = 0.3$  are adjustable model constants which representing the coalescence efficiency. The maximum allowable void fraction  $\alpha_{\max}$  takes the value of 0.8 which considers the point of transition from slug to annular flow.

The rate of bubble break-up is expressed as:

$$\phi_n^{TI} = F_B C_{TI} \frac{\alpha_g \varepsilon^{1/3}}{D_S^{11/3}} \left( 1 - \frac{We_{cr}}{We} \right) \exp\left(-\frac{We_{cr}}{We}\right) \quad (6)$$

Furthermore, by assuming spherical bubbles travel with its terminal velocity, the rate of collision caused by wake entrainment is then formulated as:

$$\phi_n^{WE} = -C_{WE} U_r \frac{\alpha_g^2}{D_S^4} \quad (7)$$

where  $C_{WE} = 0.0073$  is a model constant which accounts for the effective wake length and the coalescence efficiency. The terminal velocity of bubbles,  $U_r$ , is given by:

$$U_r = \left( \frac{D_S g \Delta \rho}{3 C_D \rho_l} \right)^{1/2} \quad (8)$$

From the above expression,  $C_{TI1} = 0.0945$  and the critical Weber number  $We_{cr} = 2.0$ , which governs the criterion of breakage, are adjustable parameters.

#### Hibiki and Ishii (2002) Model

Different from Wu et al. (1998), Hibiki and Ishii (2002) believed that wake entrainment is only significant between pairs of large cap bubbles in viscous fluid, the effect of the wake entrainment coalescence for spherical dispersed bubbles was therefore negligible. Assuming that the bubble movement behaves analogously to ideal gas molecules, the coalescence rate and breakup rate can be determined as follow:

$$\phi_n^{RC} = -F_C C_{RC1} \frac{\alpha_g^2 \varepsilon^{1/3}}{D_S^{11/3} (\alpha_{max} - \alpha_g)} \exp\left(-C_{RC2} \frac{\rho_l^{1/2} \varepsilon^{1/3} D_S^{5/6}}{\sigma^{1/2}}\right) \quad (9)$$

$$\phi_n^{TI} = -F_B C_{TI1} \frac{\alpha_g^2 (1 - \alpha_g) \varepsilon^{1/3}}{D_S^{11/3} (\alpha_{max} - \alpha_g)} \exp\left(-C_{TI2} \frac{\sigma}{\rho_l \varepsilon^{2/3} D_S^{5/3}}\right) \quad (10)$$

Here, constants  $C_{RC1} = 0.03$ ,  $C_{RC2} = 1.29$ ,  $C_{TI1} = 0.03$  and  $C_{TI2} = 1.37$  are the adjustable model constants which were calibrated with a series of experimental data.

#### Yao and Morel (2004) Model

Yao and Morel (2004) have pointed out that the aforementioned two models have been developed based on two different considerations: the free traveling time or the interaction time. They argued that both characteristic times are identically important. Taking two considerations into account, the bubble coalescence rate is derived as:

$$\phi_n^{RC} = -F_C C_{RC1} \frac{\alpha_g^2 \varepsilon^{1/3}}{D_S^{11/3}} \frac{\exp(-C_{RC2} \sqrt{We/We_{cr}})}{(\alpha_{max}^{1/3} - \alpha_g)/\alpha_{max}^{1/3} + C_{RC3} \alpha_g \sqrt{We/We_{cr}}} \quad (11)$$

where the derived coefficients are  $C_{RC1} = 2.86$ ,  $C_{RC2} = 1.017$  and  $C_{RC3} = 1.922$ .

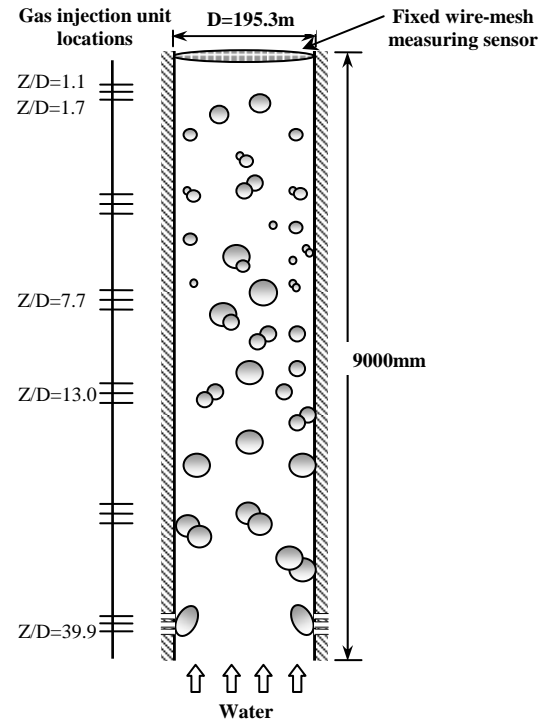
The bubble breakage rate is given by:

$$\phi_n^{TI} = F_B C_{TI1} \frac{\alpha_g (1 - \alpha_g) \varepsilon^{1/3}}{D_S^{11/3}} \frac{\exp(-We_{cr}/We)}{1 + C_{TI2} (1 - \alpha_g) \sqrt{We/We_{cr}}} \quad (12)$$

where coefficients  $C_{TI1} = 1.6$  and  $C_{TI2} = 0.42$  are the derived model constants. On top of the three different kernels, calibration factors  $F_C$  for coalescence and  $F_B$  for breakage are also included for model calibration in the three kernel models which will be discussed later on.

## EXPERIMENTAL ARRANGMENT

As discussed in previous section, with the aim to study the performance of the three different kernels in large-scale bubbly flow systems, the large scale TOPFLOW experimental data (Prasser et al., 2007) were selected for



Z: The distance between measuring position and the gas injection units

**Figure 1:** Schematic drawing of the test section of TOPFLOW experiment.

validation exercise in this article. In the TOPFLOW test facility, as depicted in Figure 1, a large vertical cylindrical pipe with the height 9000mm and inner diameter of 195.3mm was adopted as test section. Considering the coalescence rate and break-up frequency sensitively depend on the temperature caused by the effect of the surface tension, all measurements were performed at a nearly constant temperature of  $T = 30^\circ\text{C}$ . The deviations were smaller than 1 K. Different from previous bubbly flow experiment, a variable gas injection system was constructed by equipping with gas injection units at 18 different axial positions from  $Z/D=1.1$  to  $Z/D=39.9$ . Three levels of air chambers were installed at each injection unit. The upper and the lower chambers have 72 annular distributed orifices of 1mm diameter for small bubble injection; while the central chamber has 32 annularly distributed orifices of 4mm diameter for large bubble injection. A fixed wire-mesh sensor was installed at the top of the pipe where instantaneous information of gas volume fraction and bubble size distribution was measured.

**Table 1:** Selected flow conditions and the corresponding boundary conditions

	T118	T119
Superficial liquid velocity, $\langle jf \rangle$ (m/s)	1.017	1.611
Superficial gas velocity, $\langle jg \rangle$ (m/s)	0.219	0.219
$\alpha_g _{inlet}$ [%]	[17.72]	[0.120]
$D_S _{inlet}$ [mm]	[15.31]	[16.04]
Reynolds Number	270442	400412

## NUMERICAL MODELLING DETAILS

The generic CFD code ANSYS CFX 11 (2007) was employed as a platform for two-fluid flow computation. The ABND model together with the three kernels of bubble coalescence and breakage was implemented via the CFX Command Language (CCL). The Shear Stress Transport (SST) model (Menter, 1994) was adapted for liquid phase turbulence closure while the effect of bubbles on liquid turbulence was handled by the Sato's bubble-induced turbulent viscosity model. Two flow conditions with large Reynolds number and big injection bubbles TOPFLOW 118 and TOPFLOW 119 (i.e. namely T118 and T119) were selected for validation in the present study. By assuming radial symmetry for both experiments, numerical simulations could be performed on a  $60^\circ$  radial sector of the pipe with symmetry boundary conditions at both vertical sides. For the inlet boundary condition, cross-section averaged gas void fraction, bubble size distribution and sauter mean bubble diameter extracted from experimental data were specified. Details of the selected flow conditions and boundary conditions for numerical simulation were summarized in Table 1.

## NUMERICAL RESULTS ANALYSIS

One should be note that Wu et al. (1998) model, Hibiki and Ishii (2002) model were separately developed and calibrated with different experimental data. Applying these kernels to other flow conditions may requires further adjustment of model coefficients (Chen et al., 2005; Krepper et al., 2008). In the present work, aiming at

harmonizing the mechanism of bubble fragmentation and coalescence in all the three kernel modelling, calibration factors  $F_B=0.10$  and  $F_C=0.25$  were employed for all three kernels.

### *Predicted gas volume fraction during evolution process of bubble rise*

To reveal the overall performance of the model with the system, Figure 2 shows the predicted cross-sectional averaged volume fraction along axial direction in comparison to the measurement data of T118 and T119. For both test cases, although substantial difference of gas volume fraction was introduced from the air injection points (see Table 1), the revolution of gas volume fraction along the pipe was reasonably captured by all ABND models. As depicted, a roughly linearly increase of gas volume fraction was found along the pipe. This increment is mainly caused by the gas expansion which is inversely proportional to the local static pressure. In the present study, as the density of gas bubbles were modelled according to ideal gas law, the trend of gas expansion was successfully replicated by the two-fluid model. For the case T119, gas volume fraction was slightly under-predicted by the model. This could be attributed to the uncertainty of the outlet static pressure or under-estimation of hydraulic pressure drop along flow direction. Nonetheless, in general, the predicted gas volume fraction profiles were in satisfactory agreement with measurements.

### *Predicted "core peak" behaviour in the fully developed flow*

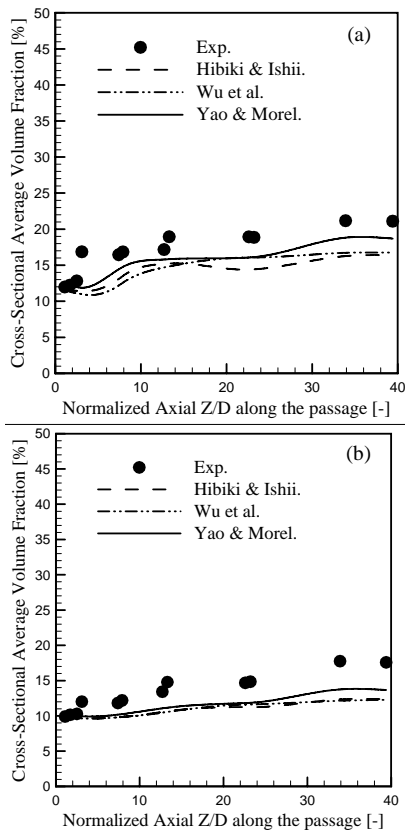


**Figure 2:** Comparison of the predicted cross-sectional averaged gas volume fraction evolutions and measurements injected at position  $Z/D=39.9$ : (a) T118; (b) T119

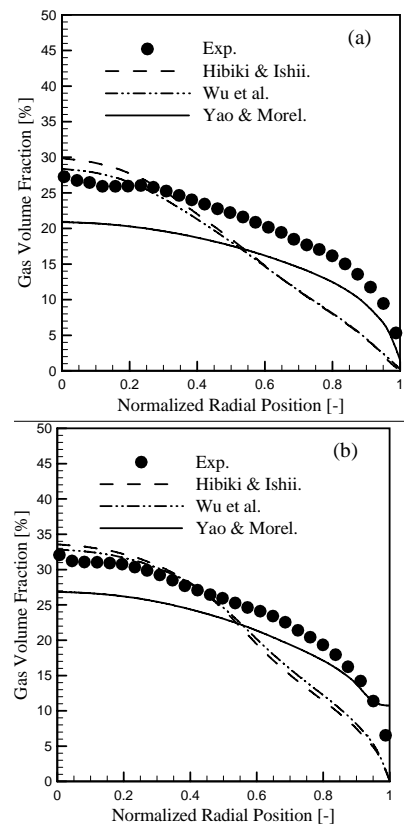


**Figure 3:** Predicted gas volume fraction distribution and measurement with injection position  $Z/D=39.9$ : (a) T118; (b) T119

With the success in capturing the overall gas expansion, a closer examination of the three kernels is then presented in the below sections. Figure 3 shows the predicted radial gas volume fraction profiles of the three kernels in comparison with the T107 and T118 measurements at the dimensionless wall injection position,  $Z/D=39.9$ . In both flow conditions, it can be observed that a well-developed “core peak” gas volume fraction profile was recorded by the measuring sensor. Such core peaking behaviour is caused by the negative lift force acting on large distorted bubbles. Driven by lift force, large distorted bubbles were then migrated toward the pipe centre forming a core peak of the gas volume fraction. As illustrated in Figure 3, the core peaking behaviour was reasonably captured by all three kernel models. Although the Yao and Morel model had considerably under-predicted the volume fractions at the pipe core, it successfully captured the main trend of the profile and compared marginally better than the other two models. On the other hand, noticeable under-estimations of Wu et al model and Hibiki and Ishii model were found at the pipe wall. As demonstrated in Figure 4, such error could be caused by the over-predictions of the sauter mean bubble diameter which sequentially generated excessive lift force pushing more bubbles towards the pipe centre.

#### Predicted bubble size distribution in the fully developed flow

The dynamical change of bubble size distribution dictates the fundamental interfacial area between gas and liquid phase; a close investigation of the dynamical changes of

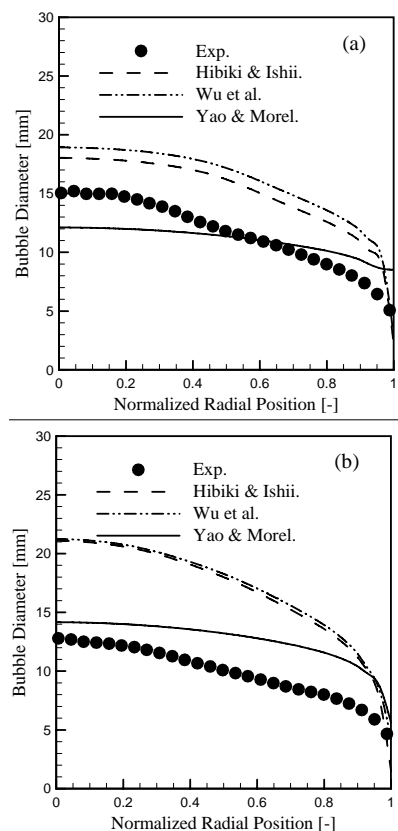


**Figure 4:** Predicted radial bubble size distribution and measurement with injection position  $Z/D=39.9$ : (a) T118; (b) T119

bubble size is certainly essential in examining its bubble coalescence and breakage kernels. Figure 4 shows the comparison between the measured and predicted radial distributions of bubble size obtained from the three kernel models. Overall, the predicted bubble size distribution of Yao and Morel model compared reasonably well with the measurements even though slightly over-predictions were found at the vicinity of wall region. Nonetheless, as discussed above, notable over-estimation can be observed when comparing the predictions of the Wu et al. model and the Hibiki and Ishii model.

#### Predicted gas velocity profiles in the fully developed flow

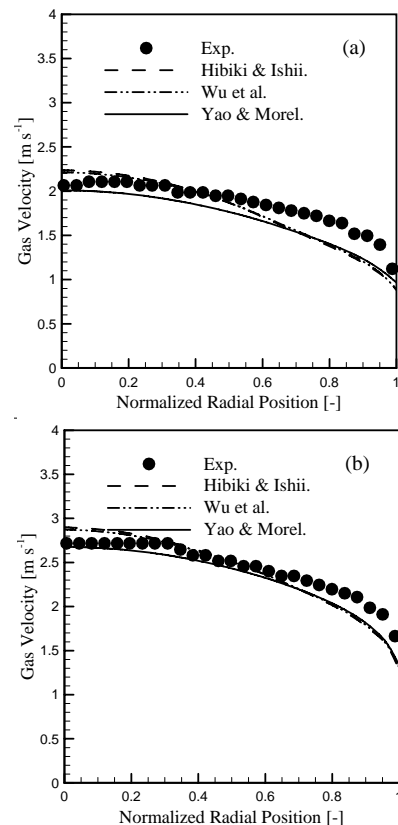


**Figure 5:** Predicted radial gas velocity profiles and measurement injected at the position  $Z/D=39.9$ : (a) T118; (b) T119

Figure 5 shows the local radial gas velocity distributions for the wall injection position of  $Z/D=39.9$ . For both test cases, as depicted, the local gas velocity behaviours had been captured remarkably well by all models. Nevertheless, for the predictions of Wu et al. model and Hibiki and Ishii model, gas velocities at the core of the pipe were slightly over-estimated. In summary, this figure further ascertains that the two-fluid model in conjunction with the population balance approach is capable to simulate the interfacial gas velocity and the effect of bubble expansion caused by pressure drop along the pipe.

## CONCLUSION

A single averaged scalar population balance approach, namely Average Bubble Number Density (ABND) model, coupled with the Eulerian-Eulerian two-fluid model is presented in this paper to handle the large-scale isothermal bubbly flows. The ABND model incorporating three

coalescence and breakage mechanisms by Wu et al. (1998), Hibiki and Ishii (2002) and Yao and Morel (2004) were compared with two individual test cases of the large-scale TOPFLOW experimental data. In general, all the three bubble mechanism kernels gave satisfactory agreement with the gas volume fraction, bubble size diameter and gas velocities measurements. In compared with other bubble mechanisms, the Yao and Morel model performed marginally superior in capturing the bubble size evolution within the large-scale bubbly flow conditions. In summary, the above comparisons verified the competence of the ABND model in modelling large-scale bubbly flows with rigorous bubble interactions. With appropriate closure to model bubble breakup and coalescence mechanism, the ABND model is capable to project the main trend of bubble size changes throughout the entire system and provide solution of some important parameters; such as: local volume fraction profile and sauter mean bubble diameter, for practical engineering usage.

#### ACKNOWLEDGEMENT

The financial support provided by the Australian Research Council (ARC project ID DP0877734) is gratefully acknowledged.

#### REFERENCES

- ANTAL, S.P., LAHEYJR., R.T. AND FLAHERTY, J.E., (1991), "Analysis of phase distribution in fully developed laminar bubbly two-phase flow", *Int. J. Multiphase Flow*, **17**, 635-652.
- BURNS, A.D., FRANK, T. AND HAMIL, I., SHI, J., (2004), "The Farve averaged drag model for turbulent dispersion in Eulerian Mult-phase flows", In: *Proceeding of the Fifth International Conference on Multiphase flow*, Yokohama, Japan.
- CFX-11, (2007), *User Manual*, ANSYS CFX.
- CHEN, P., DUDUKOVIC, M.P. and SANYAL, J., (2005), "Three-dimensional simulation of bubble column flows with bubble coalescence and breakup", *AIChE J.*, **51**, 696-712.
- CHEUNG, S.C.P., YEOH, G.H. and TU, J.Y., (2007b), "On the numerical study of isothermal vertical bubbly flow using two population balance approaches", *Chem. Eng. Sci.*, **62**, 4659-4674.
- CHEUNG, S.C.P., YEOH, G.H. and TU, J.Y., (2008), "Population balance modelling of bubbly flows considering the hydrodynamics and thermomechanical processes", *AIChE J.*, **54**, 1689-1710.
- DREW, D.A. and LAHEY JR., R.T., (1979), "Application of general constitutive principles to the derivation of multidimensional two-phase flow equation", *Int. J. Multiphase Flow*, **5**, 243-264.
- EKAMBARA, K. and DHOTRE, M.T., (2007), "Simulation of oscillatory baffled column: CFD and population balance", *Chem. Eng. Sci.*, **62**, 7205-7213.
- HIBIKI, T. and ISHII, M., (2002), "Development of one-group interfacial area transport equation in bubbly flow systems", *Int. J. Heat Mass Trans.*, **45**, 2351-2372.
- ISHII, M., (1975), "Thermo-fluid dynamic theory of two-phase flow", *Eyrolles*, Paris.
- ISHII, M. AND ZUBER, N., (1979), "Drag coefficient and relative velocity in bubbly, droplet or particulate flows", *AIChE. J.*, **5**, 843-855.
- KREPPER, E., LUCAS, D., FRANK, T., PRASSER, H.M. and ZWART, P.J., (2008), "The inhomogeneous MUSIG model for the simulation of polydispersed flows", *Nuclear Eng. and Design*, **238**, 1690-1702.
- MENTER, F.R., (1994), "Two-equation eddy viscosity turbulence models for engineering applications", *AIAA J.*, **32**, 1598-1605.
- PRASSER, H.M., BEYER, M., CARL, H., GREGOR, S., LUCAS, D., PIETRUSKE, H., SCHUTZ, P. and WEISS, F.P., (2007), "Evolution of the structure of a gas-liquid two-phase flow in a large vertical pipe", *Nuclear Eng. and Design*, **237**, 1848-1861.
- SERIZAWA, A., KATAOKA, I., Eds., (1988), "Phase distribution in two-phase flow", (p.179-224), Washington, DC: Transient phenomena in multiphase flow.
- WU, Q., KIM, S., ISHII, M. and BEUS, S.G., (1998), "One-group interfacial area transport in vertical bubbly flow", *Int. J. Heat Mass Trans.*, **41**, 1103-1112.
- YAO, W. and MOREL, C., (2004), "Volumetric interfacial area prediction in upward bubbly two-phase flow", *Int. J. of Heat and Mass Trans.*, **47**, 307-328.
- TOMIYAMA, A., (1998), "Struggle with computational bubble dynamics", *Third International Conference on Multiphase Flow*, Lyon, France.